

Copy-Move Forgery Detection and Question Answering for Remote Sensing Image

Ze Zhang[†], Enyuan Zhao[†], Ziyi Wan, Jie, Nie^{*}, *Member, IEEE*,
Xinyue Liang, *Member, IEEE*, Lei Huang, *Member, IEEE*

Abstract—This paper introduces the task of Remote Sensing Copy-Move Question Answering (RSCMQA). Unlike traditional Remote Sensing Visual Question Answering (RSVQA), RSCMQA focuses on interpreting complex tampering scenarios and inferring relationships between objects. Based on the practical needs of national defense security and land resource monitoring, we have developed an accurate and comprehensive global dataset for remote sensing image copy-move question answering, named RS-CMQA-2.1M. These images were collected from 29 different regions across 14 countries. Additionally, we have refined a balanced dataset, RS-CMQA-B, to address the long-standing issue of long-tail data in the remote sensing field. Furthermore, we propose a region-discriminative guided multimodal CMQA model, which enhances the accuracy of answering questions about tampered images by leveraging prompt about the differences and connections between the source and tampered domains. Extensive experiments demonstrate that our method provides a stronger benchmark for RS-CMQA compared to general VQA and RSVQA models. Our dataset and code are available at <https://github.com/shenyedepisa/RSCMQA>.

Index Terms—Copy-move forgery detection, tamper detection, visual question and answering, remote sensing.

I. INTRODUCTION

High-resolution remote sensing images are instrumental in rapidly acquiring critical information [1], [2]. These images can be utilized for soil moisture inversion, monitoring forest coverage, enhancing ecological protection policies, and integrating multi-source remote sensing data to depict urban development trends and strengthen urban management [3]. Additionally, extracting information from remote sensing images is crucial for national defense security monitoring, especially for situational awareness during wartime [4]. However, the content of digital remote sensing images is susceptible to manipulation or forgery, which can be achieved by copying objects from the original image to another location. Copy-move image forgery involves copying a region of the image (source domain) to another location within the same image (tampering domain). Since the tampered and source regions originate from the same image, their optical characteristics

are nearly identical, significantly increasing the difficulty of detecting the tampered areas.

Detecting tampering in remote sensing images holds significant academic and practical value. Traditional methods for copy-move forgery detection (CMFD) in natural images primarily encompass block-based, keypoint-based, and deep learning-based approaches [5]–[7]. However, the unique perspectives inherent in remote sensing images, coupled with extensive monitoring areas, numerous small-sized target objects, and limited resolution, exacerbate the challenges faced by general CMFD methods in accurately identifying tampered regions. Specifically, extracting high-level semantic information from the source and target domains in complex tampering scenarios is challenging, which further impeding researchers' ability to access and interpret these critical tampering details.

Remote Sensing Visual Question Answering (RSVQA) leverages neural networks, driven by textual inputs, to enable the perception of remote sensing images, thereby surmounting the efficiency constraints of information extraction for remote sensing interpretation tasks. Preliminary VQA methods and datasets specific to the remote sensing domain, introduced by scholars such as Lobry [8], [9], Zheng [10], and Yuan [11], have established the foundational framework for the RSVQA task. Examples of remote sensing image copy-move tampering and RSVQA tasks are shown in Figure 1. Nonetheless, in light of the practical demands of national defense security and land resource monitoring, current RSVQA methodologies fall short in their capacity to accurately extract high-level attributes, such as source and target domains in copy-move tampering scenarios. Specifically, current research is confronted with the following three challenges:

1) Neglect of Copy-Move Forgery Research: Current research in RSVQA primarily focuses on extracting information from untampered remote sensing images, lacking a question-answering system tailored for complex scenarios involving tampered images.

2) Lack of Comprehensive and Balanced Datasets: The RSVQA dataset, encompassing image-level, semantic-level, and finer-grained questions, suffers from a highly imbalanced distribution of question types, potentially introducing biases into the question-answering models.

3) Challenges in Perceiving Tampered Images: Tampered remote sensing images present significant challenges to the model's discriminative capabilities, particularly in accurately discerning the attributes and spatial relationships of source and tampered regions.

In response to this need, we introduce a large-scale Remote

This work was supported by the National Natural Science Foundation of China (U23A20320) and the National Key R&D Program of China (2023YFC3108700).

Ze Zhang, Enyuan Zhao, Ziyi Wan, Jie Nie, Xinyue Liang and Lei Huang are with the College of Information Science and Engineering, Ocean University of China, Qingdao, 266100, China.

[†]: These authors have contributed equally to this work and share first authorship.

Jie Nie is the corresponding author; Emails:niejie@ouc.edu.cn.

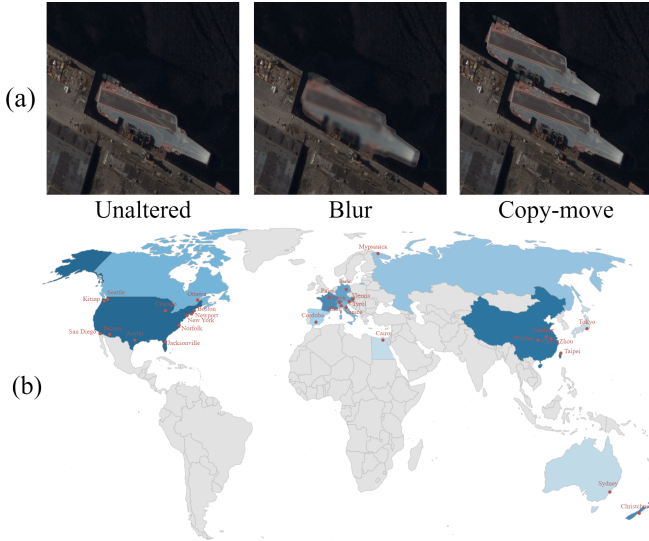


Fig. 1. (a) Example of remote sensing images being tampered with by blurring and copy-move forgery. (b) Overview of the dataset distribution.

Sensing Image Copy-Move Question Answering dataset, accompanied by a balanced subset of questions. Moreover, we propose a region association-aware framework for CMQA, designed to advance the complex RSCMQA task. The principal contributions of this work are as follows:

- We propose the RS-CMQA-2.1M dataset, which includes over 126k tampered images, combinations of source domain masks and tampering domain masks, and an additional 48k untampered images serving as negative samples. These images were meticulously collected from more than 29 regions across 14 countries. From these images, we have generated 2.1 million CM-Q-A triplets. All CM-Q-A triplets are classified into 15 distinct question categories and 54 answer types.
- Based on the RS-CMQA-2.1M dataset, we performed a weighted random sampling of all questions to eliminate category bias, and curated a balanced subset of questions, named RS-CMQA-B. Each question type in RS-CMQA-B contains 25k CM-Q-A triplets, totaling 375k CM-Q-A triplets. Notably, the distribution of answers within each question type is also balanced.
- To enable the question-answering model to perceive the key semantic features of copy-move forgery, we propose a forgery awareness framework that performs pixel-level discrimination of the source and tampering domains, providing regional prompt masks for remote sensing images and cross-modal semantic guidance for textual features. It comprehensively aggregates the prompt of the source and tampering domains for answering.

II. RELATED WORK

A. Copy Move Forgery Detection

Image copy-move forgery involves copying and relocating entities within an image to either conceal elements or emphasize objects. Traditional detection algorithms rely on strict prior knowledge of image properties and are divided

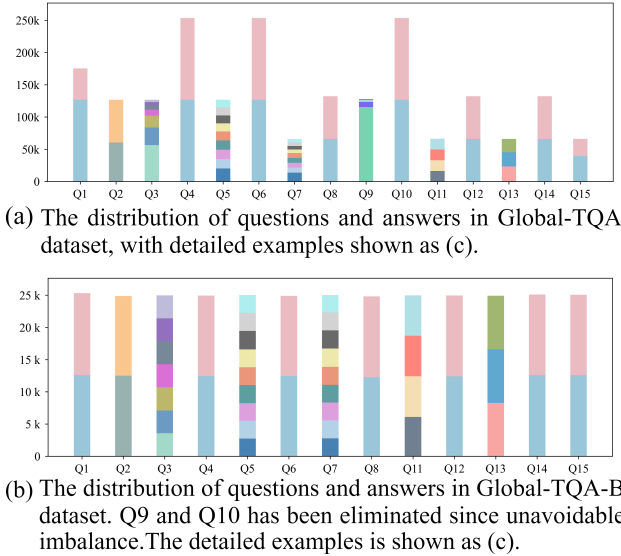
into block-based and keypoint-based methods. Block-based methods, such as Principal Component Analysis (PCA) [12], Discrete Wavelet Transform (DWT) [13], and Fourier Transform (FT) [14], require segmenting images into overlapping blocks and processing each block individually, which increases computational costs. Keypoint-based methods, including SIFT [15], SURF [16], TRIANGLE [17], and ORB [18], offer more flexible feature extraction but struggle with smooth regions lacking distinct boundaries.

Given the exponential increase in image data, manually designing priors has become impractical. Consequently, deep learning-based methods now dominate CMFD research. Busternet [19] introduced a parallel dual-branch neural network for separate detection of source and tampered domains. Chen [20] then transitioned to a serial approach to resolve feature consistency issues. Islam [21] pioneered the use of Generative Adversarial Networks (GANs) in CMFD, enhancing localization accuracy. Liu [22] combined keypoint extraction with deep learning to improve forgery localization through feature point matching. CMCF-Net [23] uses a stacked fusion model to focus on suspicious objects at different scales. UCM-Net [24] treats copy-move forgery as a semantic segmentation task, employing a multi-scale segmentation network for tampered area identification. Wang [25] proposed an approach that first estimates similar regions coarsely, followed by object-level matching between source and target domains.

Current research on copy-move forgery detection, through both traditional and deep learning methods, largely focuses on object detection, which is limiting for remote sensing images due to their noisy content. This compromises accuracy and fails to provide sufficient information. Thus, integrating copy-move forgery detection into multimodal question-answering tasks is essential. Moreover, publicly available datasets like CoMoFoD [26], COVERAGE [27], MMTDSet [28], and MICC [29] are primarily designed for natural images, highlighting the need for specialized datasets. Research on ID [30] and medical image [31] forgery detection underscores this necessity. Therefore, developing a dataset specific to remote sensing images and designing corresponding QA models is an urgent research priority.

B. Remote Sensing Visual Question Answering

The RSVQA task enables researchers to query remote sensing images using customized multimodal question-answering techniques, thereby obtaining advanced information specific to image content or spatial dependencies among visible objects. Lobery [8] introduced the initial RSVQA model. Building on this, Bazi [32] incorporated a Transformer-based VQA method. Chappuis [33] classified image information and generated textual prompts, which were then input into a language model for answer prediction. Yuan [11] proposed a language-guided approach with a soft weighting strategy to direct image attention progressively from easy to hard. Siebert [34] employed the VisualBERT model [35] to better learn joint representations. Lucrezia [36] and Wang [37] used segmentation masks to guide the model's attention to critical image information. ChangeVQA [38] detects regional changes in images captured at the same location over different time periods.



Basic questions	Q1	Has this image been tampered with?	A1: 'Yes', 'No'
	Q2	What is the type of image tampering?	A2: 'Blur', 'Copy-move'
	Q3	What types of objects have been tampered with?	A3: 'Car', 'Tree', 'Ship', 'Plane', 'Building', 'Farmland', 'Road'
	Q4	Is the tampered object a {A3}?	A4: 'Yes', 'No'
Independent questions	Q5	Where is the source domain in the image?	A5: 'Upper Left', 'Upper', 'Upper Right', 'Left', 'Middle', 'Right', 'Lower Left', 'Lower', 'Lower Right'
	Q6	Is the source domain located on the {A5} side of the image?	A6: 'Yes', 'No'
	Q7	Where is the tampered domain in the image?	A7: 'Upper Left', 'Upper', 'Upper Right', 'Left', 'Middle', 'Right', 'Lower Left', 'Lower', 'Lower Right'
	Q8	Is the tampered domain located in the {A7} of the image?	A8: 'Yes', 'No'
	Q9	How large is the area that has been tampered with?	A9: 'Zero to Five Percent', 'Five to Ten Percent', 'Ten to Fifteen Percent', 'More than Fifteen Percent'
	Q10	Does the tampered domain account for {A9} of the entire map?	A10: 'Yes', 'No'
Related questions	Q11	In which direction is the tampering domain relative to source domain?	A11: 'Upper side', 1: 'Lower side', 2: 'Left side', 3: 'Right side'
	Q12	Is the tampering domain on the {A11} of the source domain?	A12: 'Yes', 'No'
	Q13	How does the size of the tampered domain change?	A13: 'Bigger', 'Equal', 'Smaller'
	Q14	Is the tampered domain {A13} in area than the source domain?	A14: 'Yes', 'No'
	Q15	Whether the tampered domain has been rotated?	A15: 'Yes', 'No'

(c) Detailed examples of questions and answers in the dataset.

Fig. 2. Data distribution of the Global-TQA dataset and the Global-TQA-B dataset as well as details of questions and answers.

While regional change detection in remote sensing images has received attention, current research lacks the extraction of critical information from tampered regions, failing to meet the fine-grained perception needs of the RS-CMQA task.

On the other hand, high-quality publicly available datasets that support RSVQA research are relatively scarce. The first to introduce the RSVQA dataset [8] was introduced in 2020, with QA pairs derived from OSM and images sourced from Sentinel-2 and other sensors. The RSIVQA dataset [10] was automatically generated from existing classification and object detection datasets such as AID [39] and HRRSD [40]. The FloodNet dataset [41] was designed for disaster assessment, primarily focusing on the inundation of roads and buildings. EarthVQA [42] encompasses various object analysis and comprehensive analysis questions, including spatial or semantic analyses of more than three objects.

These datasets transition from simple questions to complex reasoning, advancing the multimodal remote sensing image community. However, prior studies have not addressed question-answering related to remote sensing image tampering. Additionally, remote sensing QA datasets often suffer from severe data imbalance. The RSVQA-LR dataset [8], a seminal dataset in this field, exhibits a disparity of over fortyfold between the least and most frequent question categories. Similarly, the latest research, the EarthVQA dataset [42], includes 166 different answers, with the top five answers accounting for 91% of the total questions, as illustrated in Figure 2. Such severe imbalance may introduce erroneous bias into models and affect the fairness of model evaluation. Therefore, providing tampering-based QA annotations for images, while ensuring both complexity and balance in the dataset, is a crucial focus of dataset development.

III. DATASET CONSTRUCTION

A. Global-TQA dataset

The original images for the Global-TQA dataset were selected from the LoveDA [43], IAILD [44], LAISFO [45],

Algorithm 1 TQA triples generation algorithm

Input: Untampered Images $imgs$, Instances Masks $objs$;
Output: Tampered Image img , Source Domain Mask m_s ,
 Tampering Domain Mask m_t , TQA Triple tqa

```

1: for  $img$  in  $imgs$  do
2:    $img.manualSelection()$ 
3: end for
4: for  $img$  in  $imgs$  do
5:   for  $obj$  in  $objs$  do
6:     if  $obj$  is complete and suitable in size then
7:        $m_s.create(obj).save()$ 
8:        $obj.randomCopy()$ 
9:        $obj.randomRotate()$ 
10:       $obj.randomScale()$ 
11:       $m_t.create(obj).save()$ 
12:       $img = copyMove(img,obj)$ 
13:      for  $n$  in range[1, 15] do
14:         $tqa.create(img, Q_n, A_n).save()$ 
15:      end for
16:       $img.save()$ 
17:    end if
18:  end for
19: end for

```

WHU-Building [46], DroneDeploy¹, HRSC [47], and iSAID [48] datasets. All images were cropped and resized to a resolution of 512×512 pixels. After manual screening, we obtained 48,260 high-quality remote sensing images. These images originate from at least 29 regions across 14 countries, as shown in Figure 1(b).

In this study, we selected seven types of salient targets for tampering: vehicles, airplanes, ships, buildings, roads, trees, and farmland. The chosen tampering targets are independent, separable regions occupying 0.1%-15% of the image area,

¹<https://github.com/dronedeploy/dd-ml-segmentation-benchmark>

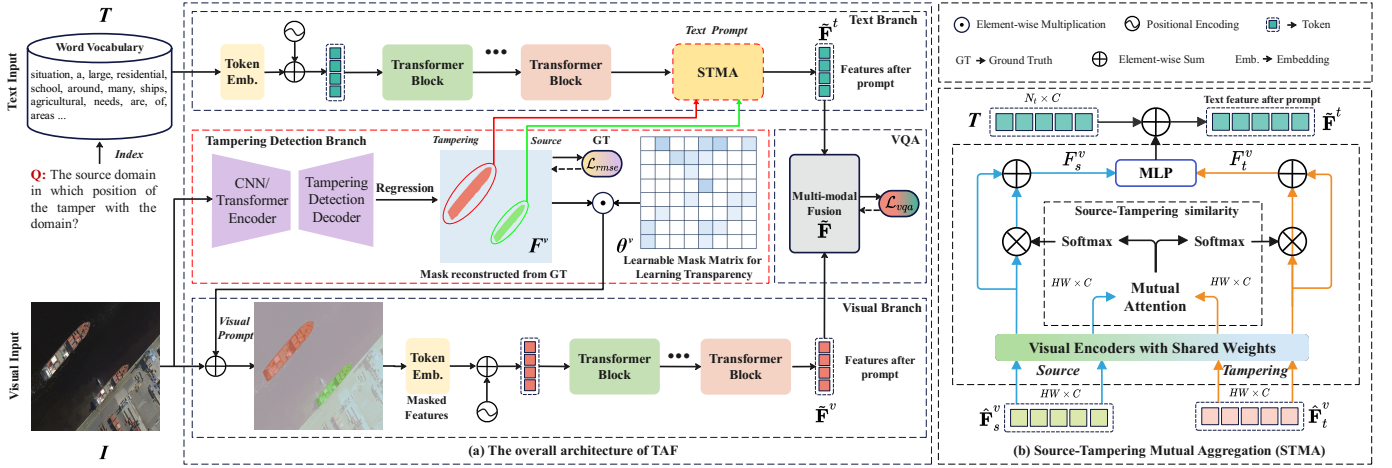


Fig. 3. An illustration of the proposed framework TAF.

ensuring that all tampered entities, except for roads, are fully presented in the images.

The tampering paradigms are divided into random blur tampering and copy-move tampering. For blur tampering, the tampered objects are randomly processed using one of three common blurring methods: Gaussian blur, mosaic blur, or oil painting smudge. The source domain and the tampering region are considered as the same area. For copy-move tampering, the tampered objects are randomly rotated and scaled between $0.5\times$ to $1.5\times$, then copied to a random location within the image. To minimize obvious overlaps between the source and tampering domains, we limited the maximum overlap ratio to 5% of the source domain, ensuring that the source and tampering domains are distinct areas. Through these algorithms and constraints, we can obtain accurate and appropriate tampered objects, source domains, and tampering domains. Based on each step of the tampering process, questions and answers are automatically generated, as shown in Algorithm 1.

In this study, a total of 2,105,839 TQA triplets were generated. The dataset was divided into training, validation, and test sets, with 70% allocated to the training set and 15% each to the validation and test sets. The Global-TQA dataset comprises 15 question categories and 54 answer types. These 15 question categories can be classified into three major types: basic questions, independent questions, and related questions, as illustrated in Figure 2(c). The distribution of questions and answers in the Global-TQA dataset is depicted in Figure 2(a). It is evident that the Global-TQA dataset is extensive yet imbalanced, presenting both opportunities and challenges for RSTQA tasks.

B. Global-TQA-B dataset

To address the long-tail issue in the dataset and provide researchers with diverse study options, we curated a balanced subset, Global-TQV-B, from the Global-TQV dataset. We excluded questions that could not eliminate category bias and performed weighted random sampling on all questions. The resulting Global-TQV-B dataset comprises 13 question types, with an average of 25,000 TQA triplets per question

type, totaling 325,007 TQA triplets. The quantity difference between various question types does not exceed 2%, and the quantity difference between answers within each question type also does not exceed 2%. The distribution of questions and answers in the dataset is shown in Figure 2(b), demonstrating that Global-TQV-B is a substantial and balanced high-quality dataset.

IV. METHODOLOGY

To identify the source and tampering domains and perform relevant reasoning, the Tampering Awareness Framework for RSTQA is designed. TAF includes a two-stage training process: 1) training a tampering detection network to generate visual and text prompts; and 2) utilizing the prompted multi-modal representations for reasoning and answering.

For the tampering detection network, masks of the source and tampering domains are used as ground truth to train the visual branch, and the output of the trained network serves as prompts for the VQA network.

A. Tamper Detection Mask for Visual Prompts

Faced with scenes containing potentially tampering regions, a reconstruction network is novelly adopted for refined guidance. Given an input image $\mathbf{I} \in \mathbb{R}^{H \times W \times 3}$, we utilize the encoder outputs $\mathbf{F}^v \in \mathbb{R}^{H' \times W' \times C}$ as visual prompts by multiplying a learnable parameter $\Theta^v \in \mathbb{R}^{H' \times W' \times 1}$ that can alter the transparency of a mask. Here, C represents the feature dimension. The prompt process is as follows:

$$\tilde{\mathbf{F}}^v = \mathbf{I} \oplus \text{MLP}(\text{Avg}(\mathbf{F}^v \odot \Theta^v)). \quad (1)$$

where $\text{Avg}(\cdot)$ signifies the average pooling operation, and $\tilde{\mathbf{F}}^v$ represents the visual representation after prompting. Compared to directly applying a learnable mask on visual features, adjusting the mask's transparency preserves the source/tampering entity's information within the visual features, preventing complete occlusion. The pixel-level visual prompts preserve the locations and semantic details inside tampering regions, contributing to the accurate detection and localization of tampered areas in images.

B. Tamper Detection Distinguish for Text Prompts

Guided by source and tampering masks, Source-Tampering Mutual Aggregation (STMA) reasons textual prompts for final answers. Specifically, through the aggregation of mutual information and the weighting of both branches, the independent channels of source and tampering domain information are ensured. Additionally, high-order information regarding the correlation between the source and tampering domains is obtained. This results in better prompts, aiding the model in understanding the semantics of both domains while distinguishing between them. The entire process is illustrated in Figure 3(b).

The inputs to STMA are the source domain reconstruction mask $\hat{\mathbf{F}}_s^v$ and the tampering domain reconstruction mask $\hat{\mathbf{F}}_t^v$, both reconstructed from the tamper detection mask. The approach involves inputting data from both modalities and casting them into two distinct roles: key and value. This dual-role transformation allows for a balanced treatment of the features derived from the source and tampering domains, enabling their effective fusion. Subsequently, the keys from both the source and tampering domains are utilized to compute the mutual attention matrix:

$$A_{mut} = \frac{1}{\sqrt{C}} \hat{\mathbf{F}}_s^v (\hat{\mathbf{F}}_t^v)^T, \quad (2)$$

where \sqrt{C} is the scale factor. Unlike general attention, which applies the attention matrix to only one branch, this variant normalizes the mutual attention matrix on both axes and applies it to the features of both the source and tampering domains. This process is cascaded through residuals, as specifically shown in the formula:

$$F_s^v = \text{Softmax}(A_{mut}) \hat{\mathbf{F}}_s^v \oplus \hat{\mathbf{F}}_s^v, \quad (3a)$$

$$F_t^v = \text{Softmax}(A_{mut}^T) \hat{\mathbf{F}}_t^v \oplus \hat{\mathbf{F}}_t^v, \quad (3b)$$

where F_s^v represents the weighted source domain branch, and F_t^v represents the weighted tampering domain branch. These are then fused together to serve as the prompt for the text representation \mathbf{T} . The prompted representation is denoted as $\tilde{\mathbf{F}}^t$, which is defined as

$$\tilde{\mathbf{F}}^t = \mathbf{T} \oplus \text{MLP}(F_s^v \oplus F_t^v), \quad (4)$$

Finally, the prompted visual representation $\tilde{\mathbf{F}}^v$ and textual representation $\tilde{\mathbf{F}}^t$ are fused for the final analysis. Additionally, various fusion methods were employed for comparative experiments during the process.

$$\tilde{\mathbf{F}} = \text{Fusion}(\tilde{\mathbf{F}}^t, \tilde{\mathbf{F}}^v). \quad (5)$$

where $\tilde{\mathbf{F}}$ is the multimodal feature that is ultimately used for VQA prediction.

C. Loss Function

The loss function \mathcal{L} is composed of tamper detection loss and VQA loss. The reconstruction loss for tamper detection is calculated based on Root Mean Squared Error (RMSE), while the VQA loss is determined using Cross Entropy (CE) loss. RMSE measures the discrepancy between the predicted source

TABLE I
COMPARED RESULTS WITH BASELINE METHODS ON GLOBAL-TQA DATASET

Method	Training	Prompt	CE	RMSE	OA(%)	AA(%)
*General Methods						
SAN	✓	×	0.6472	-	66.44	59.95
MCAN	✓	×	0.5230	-	75.32	70.45
DVQA	✓	×	0.5316	-	74.07	71.68
*Remote Sensing Methods						
RSVQA	✓	×	0.6230	-	70.17	62.78
RSIVQA	✓	Seg	0.3223	0.1306	86.75	83.04
EarthVQA	✓	Seg	0.3168	0.1187	87.34	83.46
*Multimodal Large Language Models						
LLava	×	×	-	-	8.44	8.03
LLava	×	Text	-	-	23.98	22.16
GeoChat	×	×	-	-	15.28	15.40
GeoChat	×	Text	-	-	35.21	34.73
TAF(ours)	✓	Tamper	0.2944	0.0459	91.41	89.09

TABLE II
COMPARED RESULTS WITH BASELINE METHODS ON GLOBAL-TQA-B DATASET

Method	Training	Prompt	CE	RMSE	OA(%)	AA(%)
*General Methods						
SAN	✓	×	1.1847	-	49.35	49.28
MCAN	✓	×	1.0471	-	54.13	54.21
DVQA	✓	×	1.0081	-	55.82	55.91
*Remote Sensing Methods						
RSVQA	✓	×	1.1305	-	49.16	49.07
RSIVQA	✓	Seg	0.8344	0.1406	59.48	59.89
EarthVQA	✓	Seg	0.8121	0.1387	61.72	62.35
*Multimodal Large Language Models						
LLava	×	×	-	-	7.46	7.98
LLava	×	Text	-	-	21.33	20.45
GeoChat	×	×	-	-	12.71	12.38
GeoChat	×	Text	-	-	31.49	29.56
TAF(ours)	✓	Tamper	0.7677	0.0889	65.04	65.01

and tampering domains and the ground truth. Specifically, RMSE is given by:

$$\text{RMSE} = \sqrt{\frac{1}{n} \sum_{i=1}^n (\hat{F}^v - F^v)^2} \quad (6)$$

where n denotes the number of samples, \hat{F}^v represents the ground truth mask, and F^v is the predicted mask. The Cross-Entropy Loss for VQA is expressed as:

$$\mathcal{L}_{vqa} = -\frac{1}{n} \sum_{i=1}^n y_i \log(\hat{y}_i), \quad (7)$$

where y_i denotes the ground truth answer and \hat{y}_i represents the probability predicted through the fused representation $\tilde{\mathbf{F}}$. The loss \mathcal{L} is defined as follows:

$$\mathcal{L} = \alpha \cdot \mathcal{L}_{vqa} + (1 - \alpha) \cdot \mathcal{L}_{rmse}. \quad (8)$$

where α is a trade-off coefficient.

TABLE III
EXPERIMENTAL PERFORMANCE OF DIFFERENT MODULES ON THE TAF ARCHITECTURE.

Tampering Head	Visual Head	Text Head	Global-TQA		Global-TQA-B	
			OA(%)	AA(%)	OA(%)	AA(%)
Swin	ResNet-152	LSTM	75.86	71.25	54.17	54.06
Swin	ResNet-152	BERT	88.97	85.30	62.11	62.03
Swin	ViT-B	BERT	89.54	86.53	62.34	62.42
U-net	ResNet-152	LSTM	75.33	70.24	55.09	55.16
U-net	ResNet-152	BERT	90.15	87.68	64.58	64.50
U-net	ViT-B	BERT	91.41	89.09	65.04	65.01

TABLE IV
COMPARED RESULTS OF MULTIMODAL AGGREGATION MODULES ON GLOBAL-TQA DATASET AND GLOBAL-TQA-B DATASET

Text Prompt	Global-TQA		Global-TQA-B	
	OA(%)	AA(%)	OA(%)	AA(%)
CrossAttention	88.67	85.26	61.18	61.12
Co-Attention	89.94	86.60	61.78	61.75
Bi-Attention	90.55	87.60	61.96	61.84
AAUE	90.62	88.07	62.79	62.77
OGA	90.99	87.89	63.68	63.63
STMA(ours)	91.41	89.09	65.04	65.01

V. EXPERIMENTAL RESULTS AND ANALYSIS

VI. EXPERIMENTS

Evaluation metrics. The Overall Accuracy (OA) for all questions and the Average Accuracy (AA) across all question classes are used to intuitively evaluate the model’s prediction results. We report the Cross-Entropy Loss (CE) of the model to assess its training performance. For models utilizing regional prompt, we also report the Root Mean Square Error (RMSE) to reflect the construction of regional prompt.

Experimental settings. All experiments were performed for 30 epochs with a batch size of 256 (32 batch size per device) using the Adam optimizer. The text head and visual head of the TAF utilized the CLIP [49] pre-trained BERT and ViT-B modules, respectively, while the tamper detection module employed a U-Net module. The hyperparameter α is set to 0.7. The learning rate settings are illustrated in Figure 4, with cosine annealing decay applied. The learning rate for the tamper detection module decayed from $1E-3$ to $1E-4$ over 15 epochs, while the remaining weights decayed from $5e-5$ to $1e-6$. For the encoders in the baseline models, we also used pre-trained models to ensure fairness. The learning rate for the CNN-based baseline model decayed from $1e-3$ to $1e-4$, and for the transformer-based baseline model, it decayed from $5E-5$ to $1E-6$. All experiments were performed using 8 NVIDIA RTX4090 GPUs.

A. Comparative experiments

Baseline Comparison. SAN [50], MCAN [51], DVQA [52], RSVQA [8], RSIVQA [10], and EarthVQA [42] were selected as baselines, and the performance of two open-source Multimodal Large Language Models (MLLMs), LLaVA1.5 7B [53] and GeoChat 7B [54], was tested on the RSTQA task. Among these, SAN, MCAN, and DVQA are general VQA models,

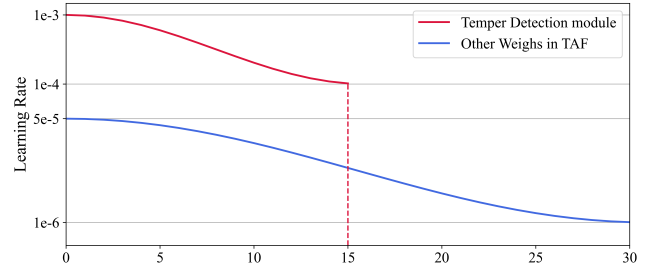


Fig. 4. Learning rate setting during TAF training

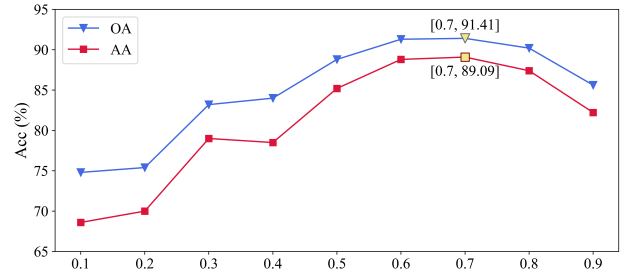


Fig. 5. Results with varied hyperparameter α .

while RSVQA, RSIVQA, and EarthVQA are designed for remote sensing VQA. Notably, RSIVQA and EarthVQA use segmentation tokens to provide visual prompt. The comparison results of TAF and baseline models on the Global-TQA and Global-TQA-B datasets are shown in Table I and Table II.

Thanks to the distinction between source and tampering domains and the prompt for visual and text features, the proposed method outperformed the second-best model by 4.7% in OA and 5.6% in AA on the Global-TQA dataset, and by 3.3% in OA and 2.6% in AA on the Global-TQA-B dataset. Overall, the four models (SAN, MCAN, DVQA, RSVQA) that did not utilize regional segmentation prompt performed poorly, while RSIVQA and EarthVQA performed relatively well. However, they did not distinguish between source and tampering domains, nor did they enhance text features. For MLLMs, although attempts were made to slightly improve the QA accuracy by adding text prompt such as detailed question guidance and limited the range of answers, the performance of MLLMs was unsatisfactory. GeoChat demonstrated a slight advantage as a remote sensing domain specific model compared to LLaVA. However, GeoChat still requires customized fine-tuning and training for RSTQA tasks and cannot be used directly as a foundational service.

All methods performed better on the Global-TQA dataset than on the Global-TQA-B dataset. This is because the Global-TQA-B dataset is smaller and more balanced, preventing models from exploiting data distribution biases, making RSTQA tasks more challenging on Global-TQA-B.

Multimodal Aggregation Module Comparison. The proposed STMA module is designed to aggregate information from both the source and tampered domains while preserving the independence of their respective features. Cross Attention [55], Co-Attention [51], Bi-Attention [56], Adaptive Aggregation of Uni-modal Experts (AAUE) [57], and Object Guided-Attention (OGA) [42] were compared with the STMA

TABLE V
RESULTS OF PROMPTS ABLATION EXPERIMENTS

Visual Prompt	Text Prompt	Global-TQA		Global-TQA-B	
		OA(%)	AA(%)	OA(%)	AA(%)
×	×	76.42	71.55	57.11	57.15
✓	×	83.07	79.26	60.09	59.98
×	✓	88.42	84.43	63.87	63.80
✓	✓	91.41	89.09	65.04	65.01

TABLE VI
RESULTS OF LOSS FUNCTION ABLATION EXPERIMENTS

MAE	RMSE	Global-TQA		Global-TQA-B	
		OA(%)	AA(%)	OA(%)	AA(%)
✓	×	89.96	85.77	61.23	61.18
×	✓	91.41	89.09	65.04	65.01
✓	✓	90.04	86.46	62.39	62.41

TABLE VII
ABLATION EXPERIMENTS FOR LEARNABLE MASK MATRIX

Learnable Mask Matrix	Global-TQA		Global-TQA-B	
	OA(%)	AA(%)	OA(%)	AA(%)
×	90.85	88.23	64.79	64.77
✓	91.41	89.09	65.04	65.01

module in terms of feature aggregation effectiveness, the results are shown in Table IV. Cross Attention is the most classical cross-modal feature aggregation method, while Co-Attention and Bi-Attention are commonly used multimodal information fusion methods in the VQA field. AAUE and OGA are recent research advancements, introduced in Manger [57] Tower and EarthVQA [42], respectively. Experimental results demonstrate that the proposed STMA module aids the model in learning the correlations and differences between the source and tampered domains, providing more comprehensive prompts for text features and improving the accuracy of question answering.

Hyperparameter settings. In the loss function, α is a hyperparameter that balances CE loss and RMSE loss. We searched for a reasonable value of α with a step size of 0.1 on the Global-TQA dataset, within the range of 0.1 to 1. The experimental results are illustrated in Figure 5. When α is set to 0.7, both OA and AA achieve the optimal value.

B. Ablation Experiments

Module Selection. Various attempts were made with the feature extraction modules used in the model, and the experimental results are presented in Table III. Swin Transformer [58] and U-net [59] were employed to generate tampering mask prompts, with the results indicating that the U-net module performed better. This may be attributed to the stronger capability of CNNs in extracting local detail features. ResNet-152 [60] and ViT-B were selected as representatives of CNN-based and Transformer-based visual encoders, respectively, with ViT-B showing a slight overall advantage. LSTM [61],

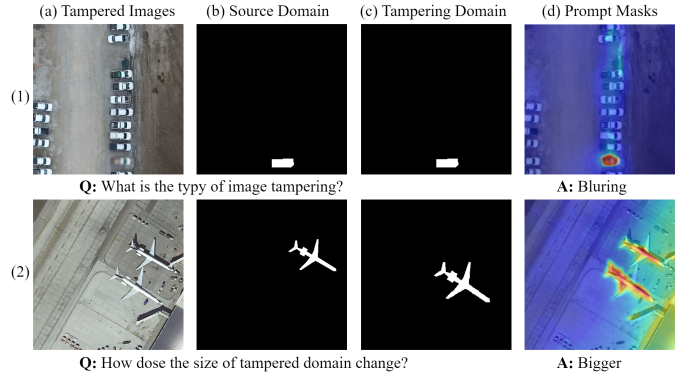


Fig. 6. Examples of images and masks from the Global-TQA dataset and examples of the RSTQA task.

and BERT were chosen as representatives of traditional text encoders and Transformer-based text encoders, respectively, with BERT demonstrating a significant advantage in this experiment. The results suggest that changes in the text head caused greater perturbations to the experimental outcomes compared to changes in the visual head.

Prompts Ablation. The source domain and tampering domain information generated by Tampering Detection Branch provides prompts for visual and textual features through prompt masks and the STMA module, respectively. Ablation experiments were conducted on these prompts, and the results are presented in Table V, showing that both types of prompts contributed positively. Notably, when using textual and visual prompts separately, the textual prompt had a greater impact on model performance. This aligns with the conclusion from the Module Selection experiment, where changes in the text head caused greater variations in the results. It is believed that semantic enhancement of textual features in RSTQA problems significantly improves question-answering performance, warranting further investigation.

Loss Function Ablation. MAE and RMSE are commonly used loss functions for regional regression, corresponding to the L1 and L2 norms in mathematics, respectively. Previous studies have shown that MAE is more robust to outliers, while RMSE is more sensitive to them. Their performance varies across different tasks [62], [63]. In the RSTQA task, using only RMSE as the loss function for the Tampering Detection Branch yields the best results, as shown in Table VI.

Learnable Mask Matrix Ablation. The Learnable Mask Matrix for learning transparency effectively regulates the impact of the mask prompt on visual features. Additionally, it alleviates unnecessary coupling between the visual prompt and the text prompt to some extent. The Learnable Mask Matrix introduces a slight yet objectively measurable improvement to the model, as demonstrated in Table VII.

C. Data Examples and Visualizations

As demonstrated in previous experiments, TAF achieved excellent performance on the Global-TQA dataset, providing accurate answers to most questions. Figure 6 presents two sets of correct question-answer examples along with the corresponding data. The Tamper Images are the input images for

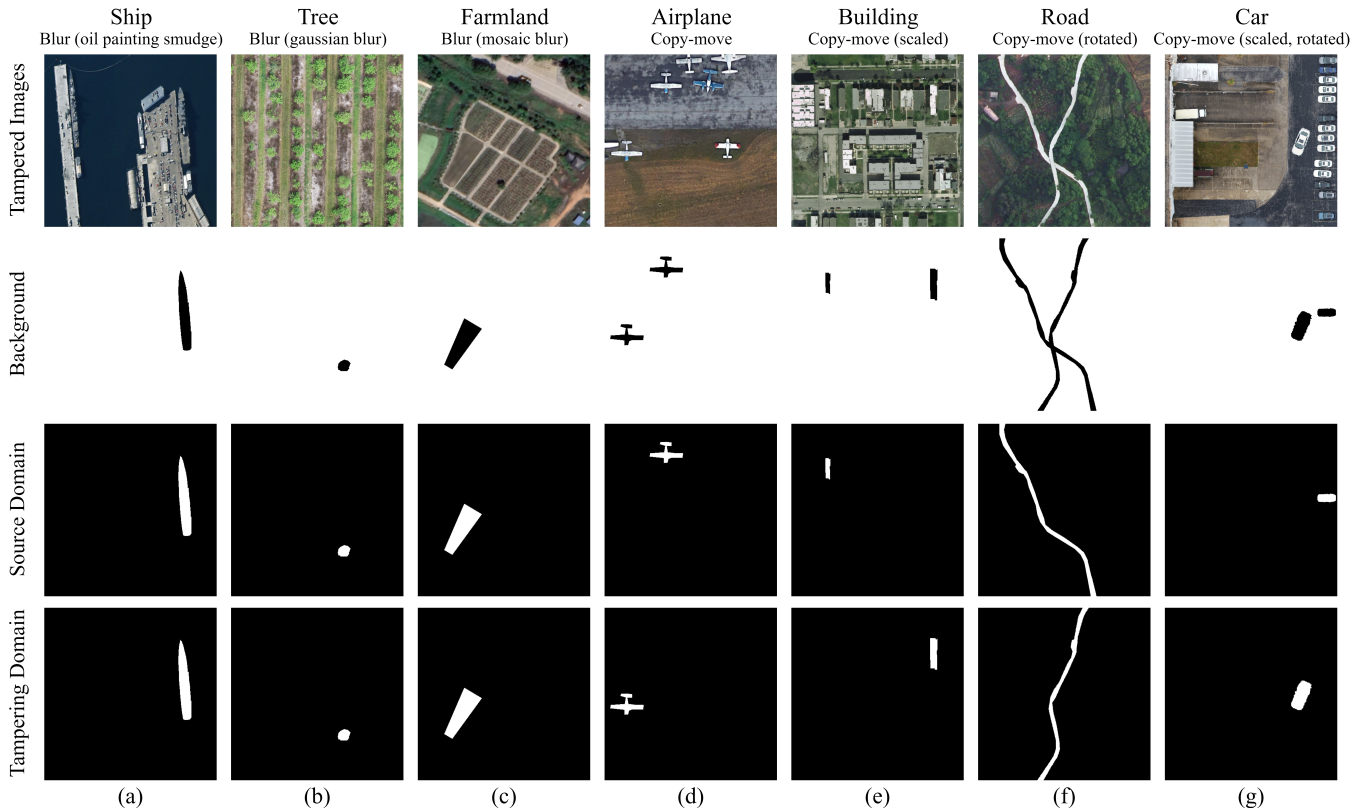


Fig. 7. Detailed examples of images in the dataset: (a) Ship tampered with oil painting smudge, (b) Tree processed with Gaussian blur, (c) Farmland processed with mosaic blur, (d) Airplane subjected to random position copy-move, (e) Building subjected to random position copy-move and scaling, (f) Road subjected to random position copy-move and rotation, (g) Car subjected to random position copy-move, scaling, and rotation.

TABLE VIII
THE QA ACCURACY OF THE TAF ON EACH TYPE OF QUESTION IN THE GLOBAL-TQA DATASET AND THE GLOBAL-TQA-B DATASET

Accuracy (%)	Basic Questions				Independent Questions						Relevance Questions					OA	AA
	Q1	Q2	Q3	Q4	Q5	Q6	Q7	Q8	Q9	Q10	Q11	Q12	Q13	Q14	Q15		
Global-TQA	96.70	99.09	77.42	90.25	86.03	94.32	94.03	96.91	99.50	99.76	87.31	93.12	76.05	83.74	62.20	91.41	89.09
Global-TQA-B	73.84	65.48	70.53	89.86	55.64	72.37	76.65	87.83	-	-	48.48	61.10	37.99	51.67	53.81	65.04	64.01

the model, while the Source Domain and Tampering Domain serve as the ground truth for RMSE loss. In instance (1), image is tampered by blurring, the Source Domain and Tampering Domain are considered the same region. In contrast, for instance (2) involving copy-move tampering, the Source Domain and Tampering Domain are clearly different. Prompt Masks represent the attention of the Visual Prompt on the image. Although not perfect, these Prompts have provided sufficiently accurate and effective information.

APPENDIX

A. Dataset Overview

Both the Global-TQA and Global-TQA-B datasets offer four types of data: tampered images, background masks, source domain masks, and tampering domain masks, as illustrated in the four rows of images in Figure 7. Figures 7 (a) to (g) respectively display seven types of tampered objects included in the dataset: ships, trees, farmland, airplanes, buildings, roads, and cars. Figures 7 (a), (b), and (c) represent blur tampering, where three image processing techniques—oil painting smudge, gaussian blur, and mosaic blur—are applied. For blur tampering, the source and tampering domains of the images are identical. Figures 7 (d), (e), (f), and (g) depict copy-move tampering. Specifically, (d) only involves random position copy-move, (e) includes random scaling of the tampered objects, (f) involves random rotation of the tampered objects, and (g) combines random scaling with random rotation of the tampered objects.

B. Experiment result analysis

Table VIII presents the question-answering accuracy of our method on the Global-TQA and Global-TQA-B datasets across various question types. Due to the extensive size of the Global-TQA dataset and the uneven distribution of questions and answers, TAF outperformed its performance on the Global-TQA-B dataset across all question types. Notably, TAF exhibited suboptimal performance when addressing relevance questions, particularly on the Global-TQA-B dataset, with a best performance of only 61.1%. This indicates that the model still faces challenges when dealing with questions that require comprehensive consideration of both the source and tampering domains, necessitating further research and improvements.

C. Subsequent updates

The experimental benchmark is based on the current version of the dataset. Future optimizations of datasets and codes will be released at <https://anonymous.4open.science/r/TQA>.

In this study, tampering detection is introduced into RSVQA, and the novel task of RSTQA is explored. We have developed a large and comprehensive multimodal dataset, Global-TQA, specifically for RSTQA, and also offer a more challenging, question-balanced dataset, Global-TQA-B, for researchers to utilize. Furthermore, we propose the Tampering Awareness Framework that provides an effective solution for the RSTQA task. Extensive experiments demonstrate the superiority of the proposed TAF. The proposed dataset and framework aim to serve as a practical benchmark for RSTQA in Earth observation scenarios. In future work, efforts will be directed towards enriching the types of questions and answers in the dataset, investigating the inferential relationship between tampering prompts and question-answering, and exploring the potential of MLLMs in optimizing the RSTQA task.

ACKNOWLEDGEMENT

This work was supported in part by the National Natural Science Foundation of China (U23A20320) and the National Natural Science Foundation of China (U22A200536).

REFERENCES

- [1] Ivan Zvonkov, Gabriel Tseng, Catherine Nakalembe, and Hannah Kerner. Openmapflow: A library for rapid map creation with machine learning and remote sensing data. *AAAI 2023*, 37(12), 2023.
- [2] Yi Xiao, Qiangqiang Yuan, Kui Jiang, Jiang He, Yuan Wang, and Liangpei Zhang. From degrade to upgrade: Learning a self-supervised degradation guided adaptive network for blind remote sensing image super-resolution. *Information Fusion*, 96, 2023.
- [3] Zhecheng Wang, Rajanie Prabha, Tianyuan Huang, Jiajun Wu, and Ram Rajagopal. Skyscript: A large and semantically diverse vision-language dataset for remote sensing. In *Proceedings of the AAAI Conference on Artificial Intelligence*, volume 38, pages 5805–5813, 2024.
- [4] Timothy M Lenton, Jesse F Abrams, Annett Bartsch, Sebastian Bathiany, Chris A Boulton, Joshua E Buxton, Alessandra Conversi, Andrew M Cunliffe, Sophie Hebden, Thomas Lavergne, et al. Remotely sensing potential climate change tipping points across scales. *nature communications*, 15:343, 2024.
- [5] Vincent Christlein, Christian Riess, Johannes Jordan, Corinna Riess, and Elli Angelopoulou. An evaluation of popular copy-move forgery detection approaches. *IEEE Transactions on information forensics and security*, 7(6):1841–1854, 2012.
- [6] Nor Bakiah Abd Warif, Ainuddin Wahid Abdul Wahab, Mohd Yamani Idna Idris, Roziana Ramli, Rosli Salleh, Shahabuddin Shamshirband, and Kim-Kwang Raymond Choo. Copy-move forgery detection: survey, challenges and future directions. *Journal of Network and Computer Applications*, 75:259–278, 2016.
- [7] Mohamed A Elaskily, Mohamed M Dessouky, Osama S Faragallah, and Ahmed Sedik. A survey on traditional and deep learning copy move forgery detection (cmfd) techniques. *Multimedia Tools and Applications*, 82(22):34409–34435, 2023.
- [8] Sylvain Lobry, Diego Marcos, Jesse Murray, and Devis Tuia. Rsvqa: Visual question answering for remote sensing data. *IEEE Transactions on Geoscience and Remote Sensing*, 58(12):8555–8566, 2020.
- [9] Sylvain Lobry, Begüm Demir, and Devis Tuia. Rsvqa meets bigearthnet: A new, large-scale, visual question answering dataset for remote sensing. In *International Geoscience and Remote Sensing Symposium*, pages 1218–1221, 2021.
- [10] Xiangtao Zheng, Binqiang Wang, Xingqian Du, and Xiaoqiang Lu. Mutual attention inception network for remote sensing visual question answering. *IEEE Transactions on Geoscience and Remote Sensing*, 60:1–14, 2022.
- [11] Zhenghang Yuan, Lichao Mou, Qi Wang, and Xiao Xiang Zhu. From easy to hard: Learning language-guided curriculum for visual question answering on remote sensing data. *IEEE transactions on geoscience and remote sensing*, 60:1–11, 2022.
- [12] M. Bashar, K. Noda, N. Ohnishi, and K. Mori. Exploring duplicated regions in natural images. *IEEE Transactions on Image Processing*, pages 1–1, 2010.
- [13] Richa Singh, Sandeep Verma, Suman Avdesh Yadav, and S Vikram Singh. Copy-move forgery detection using sift and dwt detection techniques. In *2022 3rd International Conference on Intelligent Engineering and Management (ICIEM)*, pages 338–343. IEEE, 2022.
- [14] Seniha Ketenci and Guzin Ulutas. Copy-move forgery detection in images via 2d-fourier transform. In *2013 36th International Conference on Telecommunications and Signal Processing (TSP)*, pages 813–816. IEEE, 2013.
- [15] Yanfen Gan, Junliu Zhong, and Chimam Vong. A novel copy-move forgery detection algorithm via feature label matching and hierarchical segmentation filtering. *Information Processing & Management*, 59(1):102783, 2022.
- [16] Ritesh Kumari and Hitendra Garg. An image copy-move forgery detection based on surf and fourier-mellin transforms. In *2023 International Conference on Artificial Intelligence and Smart Communication (AISC)*, pages 515–519. IEEE, 2023.
- [17] Edoardo Ardizzone, Alessandro Bruno, and Giuseppe Mazzola. Copy-move forgery detection by matching triangles of keypoints. *IEEE Transactions on Information Forensics and Security*, 10(10):2084–2094, 2015.
- [18] Gyanda Kaushal and Badal Soni. Orbcmfd: Oriented fast and rotated brief keypoints based image copy-move forgery detection. In *2024 IEEE Students Conference on Engineering and Systems (SCES)*, pages 1–5. IEEE, 2024.
- [19] Yue Wu, Wael Abd-Elmageed, and Prem Natarajan. Busternet: Detecting copy-move image forgery with source/target localization. In *Proceedings of the European conference on computer vision (ECCV)*, pages 168–184, 2018.
- [20] Beijing Chen, Weijin Tan, Gouenou Coatrieux, Yuhui Zheng, and Yun-Qing Shi. A serial image copy-move forgery localization scheme with source/target distinguishment. *IEEE Transactions on Multimedia*, 23:3506–3517, 2020.
- [21] Ashraf Islam, Chengjiang Long, Arslan Basharat, and Anthony Hoogs. Doa-gan: Dual-order attentive generative adversarial network for image copy-move forgery detection and localization. In *Proceedings of the IEEE/CVF conference on computer vision and pattern recognition*, pages 4676–4685, 2020.
- [22] Yaqi Liu, Chao Xia, Xiaobin Zhu, and Shengwei Xu. Two-stage copy-move forgery detection with self deep matching and proposal superglue. *IEEE Transactions on Image Processing*, 31:541–555, 2021.
- [23] Lizhi Xiong, Jianhua Xu, Ching-Nung Yang, and Xinpeng Zhang. Cmf-net: An end-to-end context multiscale cross-fusion network for robust copy-move forgery detection. *IEEE Transactions on Multimedia*, 2023.
- [24] Shaowei Weng, Tanguo Zhu, Tiancong Zhang, and Chunyu Zhang. Ucm-net: A u-net-like tampered-region-related framework for copy-move forgery detection. *IEEE Transactions on Multimedia*, 26:750–763, 2023.
- [25] Jingyu Wang, Niantai Jing, Ziyao Liu, Jie Nie, Yuxin Qi, Chi-Hung Chi, and Kwok-Yan Lam. Object-level copy-move forgery image detection

- based on inconsistency mining. In *Companion Proceedings of the ACM on Web Conference 2024*, pages 943–946, 2024.
- [26] Dijana Tralic, Ivan Zupancic, Sonja Grgic, and Mislav Grgic. Comofod—new database for copy-move forgery detection. In *Proceedings ELMAR-2013*, pages 49–54. IEEE, 2013.
- [27] Bihan Wen, Ye Zhu, Ramanathan Subramanian, Tian-Tsong Ng, Xuanjing Shen, and Stefan Winkler. Coverage—a novel database for copy-move forgery detection. In *2016 IEEE international conference on image processing (ICIP)*, pages 161–165. IEEE, 2016.
- [28] Zhipei Xu, Xuanyu Zhang, Runyi Li, Zecheng Tang, Qing Huang, and Jian Zhang. Fakeshield: Explainable image forgery detection and localization via multi-modal large language models. *arXiv preprint arXiv:2410.02761*, 2024.
- [29] Irene Amerini, Lamberto Ballan, Roberto Caldelli, Alberto Del Bimbo, Luca Del Tongo, and Giuseppe Serra. Copy-move forgery detection and localization by means of robust clustering with j-linkage. *Signal Processing: Image Communication*, 28(6):659–669, 2013.
- [30] Gaël Mahfoudi, Frédéric Morain-Nicolier, Florent Retraint, and Marc Pic. Cmid: A new dataset for copy-move forgeries on id documents. In *2021 IEEE International Conference on Image Processing (ICIP)*, pages 3028–3032. IEEE, 2021.
- [31] Hao-Chiang Shao, Tse-Yu Tseng, Yuan-Rong Liao, Chi-Chun Chen, Chung-Yang Hung, and Ming-Hsin Liang. Detecting biomedical copy-move forgery by attention-based multiscale deep descriptors. In *2024 IEEE International Conference on Image Processing (ICIP)*, pages 2895–2901. IEEE, 2024.
- [32] Yakoub Bazi, Mohamad Mahmoud Al Rahhal, Mohamed Lamine Mekhalfi, Mansour Abdulaziz Al Zuair, and Farid Melgani. Bi-modal transformer-based approach for visual question answering in remote sensing imagery. *IEEE Transactions on Geoscience and Remote Sensing*, 60:1–11, 2022.
- [33] c chappuis, v zermatten, s lobry, b le saux, and d tuia. Prompt-rsvqa: Prompting visual context to a language model for remote sensing visual question answering. In *Computer Vision and Pattern Recognition*, pages 1371–1380, 2022.
- [34] Tim Siebert, Kai Norman Clasen, Mahdyar Ravanbakhsh, and Begüm Demir. Multi-modal fusion transformer for visual question answering in remote sensing. *CORR*, 12267, 2022.
- [35] Liunian Harold Li, Mark Yatskar, Da Yin, Cho-Jui Hsieh, and Kai-Wei Chang. Visualbert: A simple and performant baseline for vision and language. *arXiv preprint arXiv:1908.03557*, 2019.
- [36] Lucrezia Tosato, Hichem Boussaid, Flora Weissgerber, Camille Kurtz, Laurent Wendling, and Sylvain Lobry. Segmentation-guided attention for visual question answering from remote sensing images. In *IGARSS 2024-2024 IEEE International Geoscience and Remote Sensing Symposium*, pages 2750–2754. IEEE, 2024.
- [37] Junjue Wang, Ailong Ma, Zihang Chen, Zhuo Zheng, Yuting Wan, Liangpei Zhang, and Yanfei Zhong. Earthvqnet: Multi-task visual question answering for remote sensing image understanding. *ISPRS Journal of Photogrammetry and Remote Sensing*, 212:422–439, 2024.
- [38] Zhenghang Yuan, Lichao Mou, Zhitong Xiong, and Xiao Xiang Zhu. Change detection meets visual question answering. *IEEE Transactions on Geoscience and Remote Sensing*, 60:1–13, 2022.
- [39] Gui-Song Xia, Jingwen Hu, Fan Hu, Baoguang Shi, Xiang Bai, Yanfei Zhong, Liangpei Zhang, and Xiaoqiang Lu. Aid: A benchmark data set for performance evaluation of aerial scene classification. *IEEE Transactions on Geoscience and Remote Sensing*, 55(7):3965–3981, 2017.
- [40] Yuanlin Zhang, Yuan Yuan, Yuchang Feng, and Xiaoqiang Lu. Hierarchical and robust convolutional neural network for very high-resolution remote sensing object detection. *IEEE Transactions on Geoscience and Remote Sensing*, 57(8):5535–5548, 2019.
- [41] Maryam Rahnemoufar, Tashnim Chowdhury, Argho Sarkar, Debvrat Varshney, Masoud Yari, and Robin Murphy. Floodnet: A high resolution aerial imagery dataset for post flood scene understanding. *IEEE Access*, 9, 2021.
- [42] Junjue Wang, Zhuo Zheng, Zihang Chen, Ailong Ma, and Yanfei Zhong. Earthvqa: Towards queryable earth via relational reasoning-based remote sensing visual question answering. In *Proceedings of the AAAI Conference on Artificial Intelligence*, volume 38, pages 5481–5489, 2024.
- [43] Junjue Wang, Zhuo Zheng, Ailong Ma, Xiaoyan Lu, and Yanfei Zhong. Loveda: A remote sensing land-cover dataset for domain adaptive semantic segmentation. In J. Vanschoren and S. Yeung, editors, *Proceedings of the Neural Information Processing Systems Track on Datasets and Benchmarks*, volume 1. Curran Associates, Inc., 2021.
- [44] Emmanuel Maggiori, Yuliya Tarabalka, Guillaume Charpiat, and Pierre Alliez. Can semantic labeling methods generalize to any city? the inria aerial image labeling benchmark. In *2017 IEEE International Geoscience and Remote Sensing Symposium (IGARSS)*, pages 3226–3229. IEEE, 2017.
- [45] Syed Waqas Zamir, Aditya Arora, Akshita Gupta, Salman Khan, Guolei Sun, Fahad Shahbaz Khan, Fan Zhu, Ling Shao, Gui-Song Xia, and Xiang Bai. isaid: A large-scale dataset for instance segmentation in aerial images. In *Proceedings of the IEEE Conference on Computer Vision and Pattern Recognition Workshops*, pages 28–37, 2019.
- [46] Shunping Ji, Shiqing Wei, and Meng Lu. Fully convolutional networks for multisource building extraction from an open aerial and satellite imagery data set. *IEEE Transactions on Geoscience and Remote Sensing*, 57(1):574–586, 2018.
- [47] Zikun Liu, Liu Yuan, Lubin Weng, and Yiping Yang. A high resolution optical satellite image dataset for ship recognition and some new baselines. In *International conference on pattern recognition applications and methods*, volume 2, pages 324–331. SciTePress, 2017.
- [48] Pascal Kaiser, Jan Dirk Wegner, Aurélien Lucchi, Martin Jaggi, Thomas Hofmann, and Konrad Schindler. Learning aerial image segmentation from online maps. *IEEE Transactions on Geoscience and Remote Sensing*, 55(11):6054–6068, 2017.
- [49] Alec Radford, Jong Wook Kim, Chris Hallacy, Aditya Ramesh, Gabriel Goh, Sandhini Agarwal, Girish Sastry, Amanda Askell, Pamela Mishkin, Jack Clark, et al. Learning transferable visual models from natural language supervision. In *International conference on machine learning*, pages 8748–8763. PMLR, 2021.
- [50] Zichao Yang, Xiaodong He, Jianfeng Gao, Li Deng, and Alex Smola. Stacked attention networks for image question answering. In *Proceedings of the IEEE conference on computer vision and pattern recognition*, pages 21–29, 2016.
- [51] Zhou Yu, Jun Yu, Yuhao Cui, Dacheng Tao, and Qi Tian. Deep modular co-attention networks for visual question answering. In *Proceedings of the IEEE/CVF Conference on Computer Vision and Pattern Recognition*, pages 6281–6290, 2019.
- [52] Zhiqian Wen, Guanghui Xu, Mingkui Tan, Qingyao Wu, and Qi Wu. Debaised visual question answering from feature and sample perspectives. *Advances in Neural Information Processing Systems*, 34:3784–3796, 2021.
- [53] Haotian Liu, Chunyuan Li, Yuheng Li, and Yong Jae Lee. Improved baselines with visual instruction tuning. In *Proceedings of the IEEE/CVF Conference on Computer Vision and Pattern Recognition*, pages 26296–26306, 2024.
- [54] Kartik Kuckreja, Muhammad Sohail Danish, Muzammal Naseer, Abhijit Das, Salman Khan, and Fahad Shahbaz Khan. Geochat: Grounded large vision-language model for remote sensing. In *Proceedings of the IEEE/CVF Conference on Computer Vision and Pattern Recognition*, pages 27831–27840, 2024.
- [55] Ashish Vaswani. Attention is all you need. *arXiv preprint arXiv:1706.03762*, 2017.
- [56] Jin-Hwa Kim, Jaehyun Jun, and Byoung-Tak Zhang. Bilinear attention networks. *Advances in neural information processing systems*, 31, 2018.
- [57] Xiao Xu, Bei Li, Chenfei Wu, Shao-Yen Tseng, Anahita Bhiwandiwala, Shachar Rosenman, Vasudev Lal, Wanxiang Che, and Nan Duan. Managertower: Aggregating the insights of uni-modal experts for vision-language representation learning. *arXiv preprint arXiv:2306.00103*, 2023.
- [58] Ze Liu, Yutong Lin, Yue Cao, Han Hu, Yixuan Wei, Zheng Zhang, Stephen Lin, and Baining Guo. Swin transformer: Hierarchical vision transformer using shifted windows. In *Proceedings of the IEEE/CVF international conference on computer vision*, pages 10012–10022, 2021.
- [59] Olaf Ronneberger, Philipp Fischer, and Thomas Brox. U-net: Convolutional networks for biomedical image segmentation. In *Medical image computing and computer-assisted intervention—MICCAI 2015: 18th international conference, Munich, Germany, October 5-9, 2015, proceedings, part III 18*, pages 234–241. Springer, 2015.
- [60] Kaiming He, Xiangyu Zhang, Shaoqing Ren, and Jian Sun. Deep residual learning for image recognition. In *Proceedings of the IEEE conference on computer vision and pattern recognition*, pages 770–778, 2016.
- [61] Sepp Hochreiter and Jürgen Schmidhuber. Long short-term memory. *Neural computation*, 9(8):1735–1780, 1997.
- [62] Cort J Willmott and Kenji Matsuura. Advantages of the mean absolute error (mae) over the root mean square error (rmse) in assessing average model performance. *Climate research*, 30(1):79–82, 2005.

- [63] Tianfeng Chai and Roland R Draxler. Root mean square error (rmse) or mean absolute error (mae)?—arguments against avoiding rmse in the literature. *Geoscientific model development*, 7(3):1247–1250, 2014.



Ze Zhang is currently pursuing a master's degree with the Faculty of Information Science and Engineering, Ocean University of China, Qingdao, China. His research interests include multimedia reasoning, especially in VQA.



Enyuan Zhao received a B.S. in electronics and information engineering from Northeast Agricultural University, China, and an M.S. in computer science and technology from Harbin Engineering University, China, in 2021. He is pursuing a Ph.D. with the Faculty of Information Science and Engineering at the Ocean University of China. His research interests include deep learning and intelligent multimodal systems.



Ziyi Wan is currently pursuing a master's degree with the Faculty of Information Science and Engineering, Ocean University of China, Qingdao, China. Her research interests include multimedia reasoning, especially in VG and VQA.



Jie Nie (Member, IEEE) received a Ph.D. in Computer Science from Ocean University of China, Qingdao, China, which she obtained in 2011. She furthered her academic pursuits as a Visiting Scholar at the School of Electrical Engineering, University of Pittsburgh, Pennsylvania, USA, from September 2009 to September 2010. Following her doctorate, she conducted post-doctoral research at Tsinghua University, Beijing, China, from 2015 to 2017. Her research focuses on social media and multimedia content analysis.



Xinyue Liang (Member, IEEE) received her B.S. degree in Communication Engineering from Beijing Jiaotong University in 2014. From 2014 to 2021, she pursued her Master's and Ph.D. degrees at the Royal Institute of Technology in Sweden. She is currently a lecturer with Ocean University of China in 2022. Her research interests are distributed machine learning, marine big data analytics, and distributed signal analysis.



Lei Huang (Member, IEEE) is professor in Ocean University of China. He obtained his Ph.D. from the Institute of Computing Technology, Chinese Academy of Sciences in 2013. His current research focuses on multimedia content analysis and retrieval, machine learning, and intelligent information processing.